

Multi-wavelength Observations of the solar eruptive activity

Brigitte Schmieder¹

¹Observatoire de Paris-Meudon, LESIA, France
email: brigitte.schmieder@obspm.fr

Abstract. We review what we have learnt about flares and prominences using multi-wavelength observations in the perspective of testing theoretical models.

1. Introduction

The emission of the Sun in activity covers a large range of wavelengths of the electromagnetic spectra from radio wavelength (decametric) to γ ray at 10^{-3} Å. Multiwavelength observations of the active sun needs the use of telescopes on the ground and in space. Only few wavelength windows are open to the ground observers: the visible light with the classical telescopes (i.e. the European Observatory, Kitt Peak in US, Hida in Japon) and the radio domain with radiotelescopes (i.e. Nanay, Zurich, Nobeyama). The other domains are reached only with instruments aboard space missions (SOHO, Yokoh, TRACE, RHESSI, WIND).

When you are observing in multi-wavelength a first task is to co-align the observations. The ground telescopes have generally no information of pointing and the pointing of the satellites is not always reliable. Different techniques of co-alignment are available based on physical properties of solar structures (i.e. darkness of sunspot in visible light, brightness of magnetic regions) or using software based on satellite pointings, cross-correlation, search of the limb of the Sun and then the center, rotation of the images with three points.

2. Flare general view

The activity of the Sun is governed by its magnetism. The solar magnetic field origine is in the sublayer below the convective zone, called “the tachocline”. As the magnetic field emerges, it is observed as pores or sunspot in visible light. During the emergence of flux, a hierarchy of loops at different altitudes is observed (Pariat *et al.* 2004). Cool loops of Arch filament System are overlaid by hot coronal loops (Figure 1).

The solar atmosphere is structured by multiple magnetic loops, anchored in sunspot umbra or in magnetic network which covers all the Sun, surrounding convective cells or supergranules ($\phi = 30$ Mm). While subphotospheric motions (differential rotation, convection) are stretching the solar surface, loops become stressed and twisted. Thus energy is stored in coronal loops. Such a stress is visible in Yokoh images of active regions which have commonly a sigmoid shape when observed on the disk (Figure 2). Magnetic energy is transformed into heating and kinetic energy (motions, particle acceleration) during reconnection of loops in the flaring process. Thus the energy needed to power the flares comes from the coronal magnetic field. The stored energy is released with emission of particles (protons, electrons, neutrons) and radiation. Such energy release is efficient only at very small scale through reconnection mechanisms (see section 4).

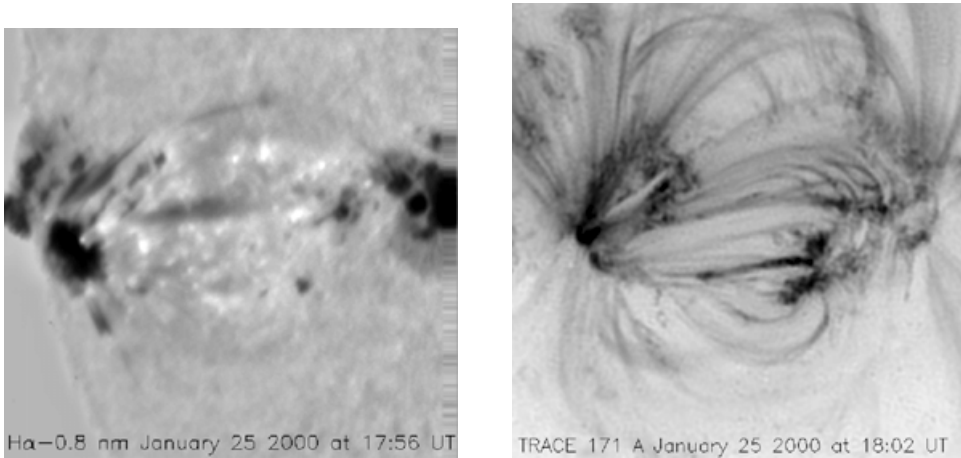


Figure 1. Loops visible during the emergence of magnetic field from the subphotosphere, left panel cool rising loops (AFS) seen in Flare Genesis experiment image in $H\alpha$ -0.8 Å right panel coronal loops observed by TRACE at 195 Å (Pariat *et al.* 2004).

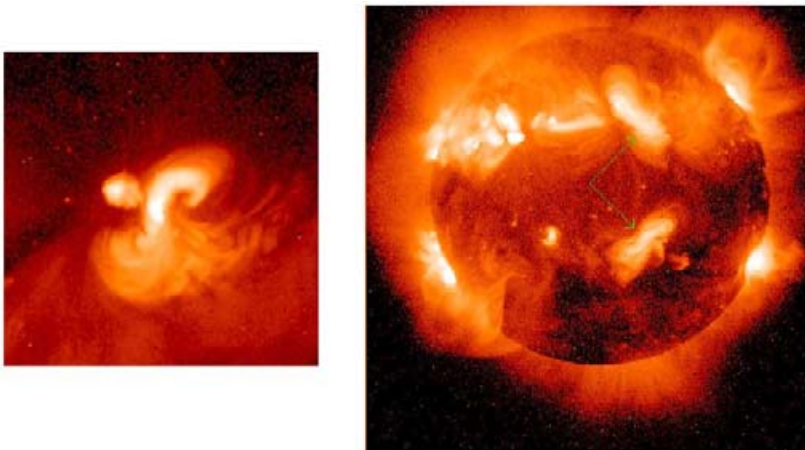


Figure 2. Active regions with a sigmoid-shape observed by Yohkoh (Fan and Gibson 2004).

Particles escape and are accelerated, bombarding downward the dense atmosphere: it is what we call the non-thermal mechanism in a flare. The plasma is heated either by this bombardment with a fast time scale (sec. or fraction of sec.) or by thermal conduction with a time scale of the order of the minute if the thermal gradient is large enough, like in the transition zone. Classical flares with enhanced of brightness are observed in visible light (white light flare), in $H\alpha$, in transition region and coronal lines (SOHO/EIT, TRACE 195 Å, 171Å, Yohkoh). This brightness corresponds to emission of radiation at different temperatures (5 to 30 MK).

The released energy range of flares is extended from 10^{26} ergs for nano/micro flares to 10^{32} ergs for large flares. The classification of flares which emitted soft X ray radiation is nanoflare, subflare A B C, medium flare M, large flare X. X1 to X27 (the largest one) flares have been observed recently on October 26-28-29 2003, January 17 and 20 2005, September 7 to 16 2005. The large flares are commonly long duration flares, they are described with 3 phases, preflare phase with opening of the overlaying loops, the main flare with reconnection and acceleration of particles (observed by RHESSI) and the last

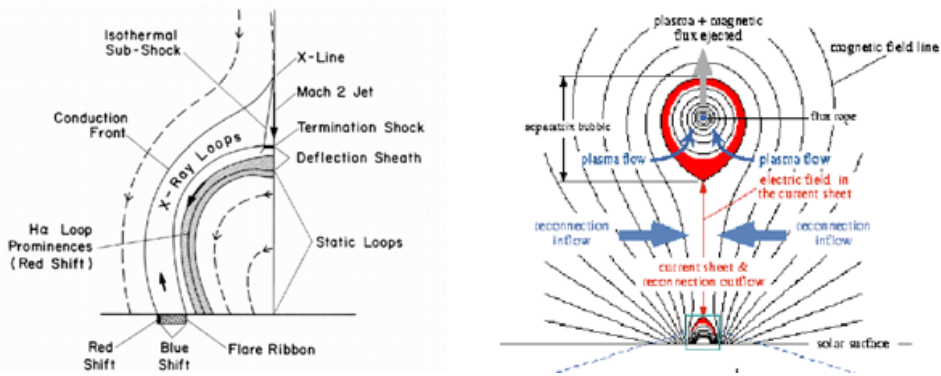


Figure 3. left panel: model of reconnection after flares and formation of two ribbons and post-flare loops (Schmieder *et al.* 1987), right panel: model of ejection of magnetic plasma and flux in the high corona (Lin and Forbes 2000).

phase or gradual phase which can last 10 hours. These three phases correspond to the classical observation of filament eruption with reconnection of loops and formation of loops so-called post-flare loops below the reconnection point (Figure 3). The loops are cooling from 30 MK to 10^5 K. The chromosphere is heated leading to the formation of well visible two ribbons that are the footpoints of the loops (Figure 4). The ribbons are travelling away from each other with a deceleration velocity.

When the flare is eruptive, ejections of plasma and development of coronal mass ejections (CMEs) are observed in the corona (SOHO/LASCO).

3. High energy particles and Radio emission of flares

The most quantitative diagnostics of energetic particles interacting at the Sun are provided by “Hard X-Ray/ γ -Ray” (HXR/GR) observations which give information on electron and ion energy spectra, numbers and energy contents (RHESSI, see the review of Vilmer, 2006). Complementary observations of the HXR bremsstrahlung emitting electrons are provided by the radio emission produced in the whole frequency range from 100 GHz to 100 MHz. Radio emissions at metric/decimetric wavelengths (i.e. in the 100 MHz–1 GHz range) most commonly produced by coherent plasma radiation mechanisms are a sensitive diagnostics of electrons of a few tens of keV injected upwards and downwards in the corona from the acceleration sites. The combination of HXR observations with spatially resolved observations in the metric/decimetric wavelengths provide information on the development of the active phenomena: on electron acceleration and transport in the corona obtained by combining X-ray spectra and images with radio images obtained with the Nançay Radioheliograph in the 450 MHz–150 MHz range (Figure 4).

Some indirect evidence of electron acceleration sites in the corona come from broad band radio spectrographic observations. Electron beams propagating along magnetic field lines in the corona produce coherent radio emissions at the local plasma frequency or its harmonic. The emitted radio bursts (type III bursts or reverse type III bursts) will exhibit characteristic frequency drifts either towards lower, resp. higher frequencies if the beam propagates in the direction opposite to the ambient electron density gradient (upwards), resp. in the direction of the gradient (downwards).

Some observations of X-ray flare suggest indeed that energy release appears near the top of 10^4 km magnetic loops possibly in the cusp region where the reconnection occurs

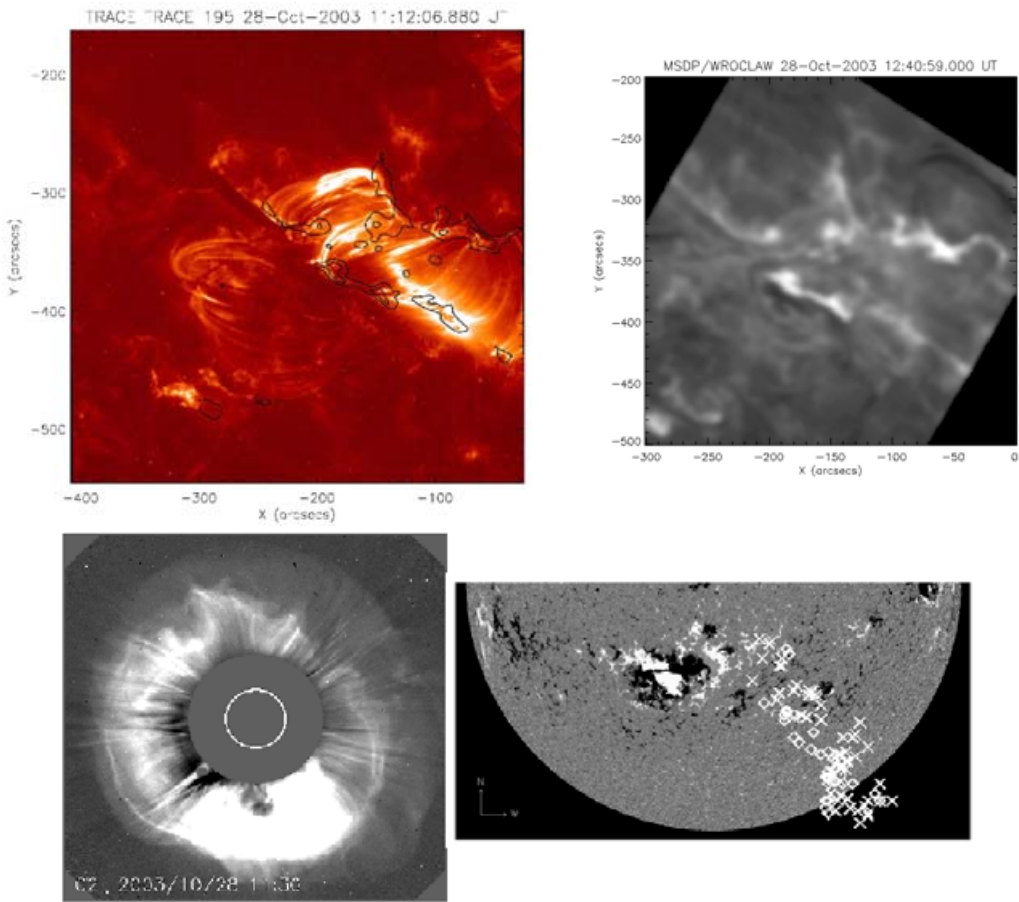


Figure 4. top panels: X17 flare observed on October 28 2003, (left panel) TRACE 171 Å with the contours of ribbons, (right panel): H α observations of the ribbons (courtesy of P.Rudawy), bottom left panel: CME as seen by LASCO, right panel: type III bursts measured at 236 and 164 MHz during a 50 sec period indicating a propagation velocity of 2500 km/s overlaying a MDI magnetogram showing the active region source of the CME and the flare (Pick *et al.* 2005).

(Sui *et al.* 2003). An other possible site of energy release is close to the interaction region between loops or loop systems of different sizes (10^4 – 10^5 km). This may indicate the formation of a current sheet between the top of flare loops and the coronal source thus bringing new observational evidence for magnetic reconnection and cusp geometry in flares.

Ejections of hot plasma as jets or plasmoids are associated with electron beam production. Soft X-ray (SXR) ejecta or rising loops (700–900 km/s) may also drive large scale coronal shocks seen as radio type II bursts. During their propagation in the corona, SXR ejecta can also be the source of electron acceleration giving rise to slowly (frequency) drifting decimetric/metric pulsating structure (Khan *et al.*, 2002). The close location of the radio pulsating structure at 327 MHz with the upper part of the SXR plasmoid strongly suggests that the acceleration is linked to the propagation of plasmoid (Figure 3).

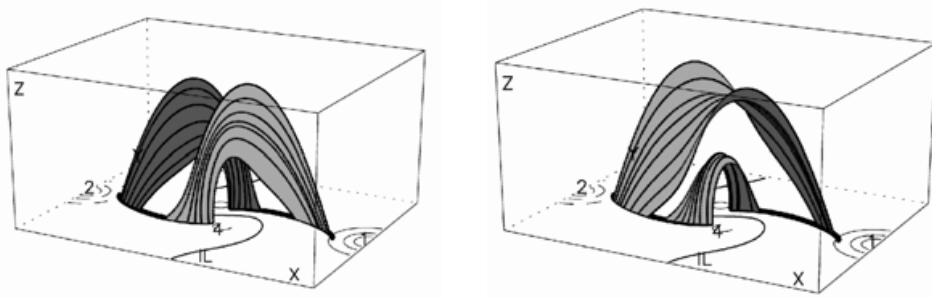


Figure 5. Perspective view of a simple configuration formed by four photospheric field concentration showing magnetic field lines mapping quasi-separatrices (QSL) before (right) and after reconnection (left). The foot prints of the QSL on the lower boundary are in thick black lines and are regions of the flare ribbons (Démoulin *et al.* 2005).

4. Magnetic topology of flaring active regions

In the solar corona, ideal MHD can be generally applied. Plasma and magnetic field are frozen in. But when E_{\parallel} is different of zero, the magnetic field can be diffused and change of connectivity of field lines through magnetic reconnection. The magnetic configuration is changed. Current layers are formed in high gradient of magnetic field regions. These regions are the sites of possible energy release.

Magnetic configurations with a complex topology, i.e. with separatrices, are the most obvious configurations where current layers can form (see the review of Démoulin (2005) for details). Separatrices are magnetic surfaces where the magnetic field line linkage is discontinuous. The simplest example is a 2-D magnetic configuration with an X-point (where the magnetic field vanishes). Two separatrices cross at the X-point, and they define four separated regions, connectivity domains, where the magnetic connectivity change continuously for one field line to its neighbor. These separatrices can be also associated to field lines tangent to its lower boundary (the photosphere) at locations called “bald patches”. The two cases have a generalization in 3-D magnetic configurations: separatrices are formed by field lines which thread either null points or bald patches.

Testing the above theory for the spatial localization of energy release sites needs the computation of the coronal magnetic field from observed photospheric magnetograms. It also needs the clearest indirect evidences of energy release (e.g. flare ribbons and loops). Some of the studied active regions have a magnetic null point in the extrapolated coronal field. The magnetic null point is weakly sensitive to perturbations of the magnetic configuration (e.g. modifying the photospheric magnetogram, or the coronal currents) when the three eigenvalues are comparable. The found null points can be at any location along the separator (intersection in 3D of the separatrices). They can be located at the top or close to the photosphere. Bald-patch separatrices have been related to the spatial location of various brightenings. Up to now only bald patches were found in minor events: small flare (Aulanier *et al.* 1998), surge (Mandrini *et al.* 2002), Ellerman Bomb (Pariat 2004).

The study of separatrices has started with the modelling of the observed photospheric magnetic field by discrete magnetic sources (charges or dipoles). The magnetic null points present between these sources are implicitly at the origin of a complex topology. These studies were extended to the presence of many sources (Démoulin *et al.* 1994). In these

cases many separatrices are present and the sources should be gathered in groups. A region where the same two groups are found, define a connectivity domain. It represents what now we called a “source model”. This model has been developed recently by Longcope as the magnetic charge topology model (MCT). The magnetic topology can become rapidly complex as the number of null points increases (Longcope and Klapper 2002).

An other approach to define the magnetic topology is to consider directly the observed magnetogram. A consequence is that there is not necessarily separatrices to interpret brightenings but a generalization of the concept of separatrices does provide an interpretation in the framework of a 3-D reconnection. Démoulin *et al.* (1996) generalized the notion of separatrices by defining the quasi-separatrices with a finite thickness (Figure 5). A high gradient is present. The main QSL properties, as derived from the analysis of several flares and theoretical configurations are the following. In the corona, local physical processes, like resistivity or kinetic processes, broaden any current region with a finite width. For the physical evolution of coronal field there is no basic difference between a separatrix and a QSL as far as the QSL is thinner than the sizes given by the “microscopic” physics. This method has been very successful to explain the shape of flare ribbons and define the location of the reconnection (Schmieder *et al.* 1997, Démoulin *et al.* 1997, Berlicki *et al.* 2004). As we modify the magnetic field at the boundary the spatial location of QSLs is smoothly changing (Aulanier *et al.* 2005). The QSLs are defined by the global properties of the magnetic configuration rather than by local ones as for the magnetic nulls and bald patches. Concentrated electric currents have been found at the borders of QSLs in studied flares (Démoulin *et al.* 1997). With QSL we do not find null points by definition. It was confirmed by observations, we have found flares with no null points (Mandrini *et al.* 2006).

5. Prominence/Filament

The prominence plasma contains 90 % of hydrogen which is partially ionized in the coolest parts (6000–8000 K) surrounded by a transition zone. They appear as dark structures on the disk in $H\alpha$ due to the absorption of the lines (depending on the source function and the optical thickness of the prominence plasma). Prominences on the limb are observed as bright structures. It is the result of the emission radiation due to scattering incident solar radiation by the coolest part of the prominence.

Coronal mass ejections are episodic expulsions of mass and magnetic field from the corona into the interplanetary medium. They reflect a high level of activity in the solar atmosphere (see review of Schmieder and van Driel 2004). However, the span of CME activity is much longer and extends well into the decay phase of active region evolution when the magnetic field is dispersed and the region is classified as quiet solar region containing filament (van Driel-Gesztelyi *et al.* 1999). Subramanian and Dere (2001), based on a sample of 32 CMEs, found that 85% of them were associated with active regions and 15% with so-called quiet regions. They found that 44% of these CMEs were associated with eruption of an active region filament and the 15% coming from “quiet” regions were all associated with filament eruption. These results are in good agreement with other statistical analyses of more numerous events having a narrower multi wavelength coverage (Saint Cyr and Webb, 1991; Webb, 1998; Zhou *et al.* 2003).

$H\alpha$ prominences have a thin volume whose thickness, length and height are respectively 5, 100, 40 Mm and taking a mean proton density of the order of 10^{10} to 10^{11} cm^{-3} then the typical mass range is $3 \times 10^{14-15}$ g so eruptive filament may account for a negligible fraction of the total mass of their related CMEs. On the other hand it has been demonstrated recently the mass of $H\alpha$ filament can be multiplied by two if we take

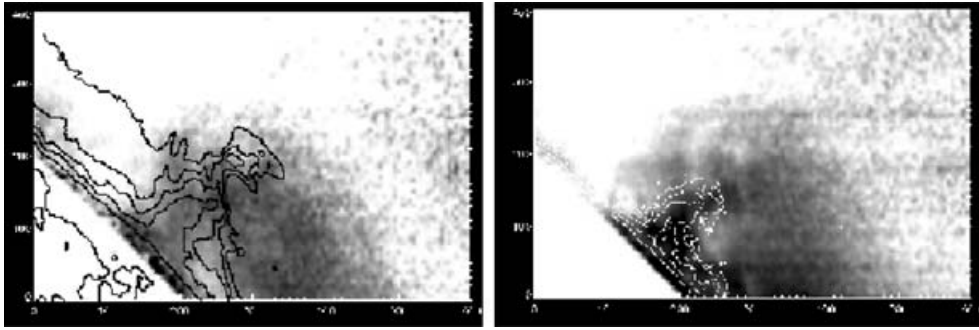


Figure 6. Prominence observed in EUV lines (Fe XII 1242 Å in the left panel and Mg X 624 Å in the right panel) overlaid by contours of cool lines (NV 1238 Å and SII 1250 Å) (Heinzel *et al.* 2006).

into account the lateral extension of the H α filament. This extension is cool plasma with a small optical thickness in H α line that did not allow to see it in H α images. It corresponds to a low contrast (<0.1). This has been discovered in Skylab observation (1973) and since explained in different steps. It was demonstrated firstly that for coronal lines having a wavelength below the hydrogen Lyman-continuum head at 912 Å the emission is weaker at the prominence location compared to the surrounding corona (Kucera *et al.* 1998, Schmieder *et al.* 1999). Then it was recognized that the absorption by the hydrogen Lyman continuum was the agent of such dimming, however this mechanism cannot be the only phenomena involved because dark filament channels are also observed in coronal lines 195 and 171 Å. The total thickness of the prominence is equal to:

$$\tau = \sigma_H N_{HI} + \sigma_{HeI} N_{HeI} + \sigma_{HeII} N_{HeII}$$

where N_{HI} is the column density of neutral hydrogen and N_{HeI} and N_{HeII} are those of neutral and singly ionized helium respectively. The ratio between the optical thickness in H α compared to the thickness of H Lyman continuum is large 20 to 100, but with the He Lyman continuum, the ratio is close to one. So the absorption mechanism is not efficient to explain the large filament channel in the TRACE 195 Å images. We propose an other mechanism called “the volume blocking”. It is a mechanism based on the fact that the volume occupied by cool material in voids around the prominence does not emit in coronal lines which are formed in much higher temperature and leads to the lowering of the coronal brightness at the prominence location relative to surrounding quiet corona. The comparison between images in the Fe XII 1242 Å and MgX 624 Å lines observed respectively by SOHO/SUMER and CDS at the limb show that similar pattern (Figure 6). That means that for Mg X the absorption mechanism is at work and for Fe XII (this line lies above the Lyman continuum head) it is the other mechanism, the absorption being inefficient at this wavelength.

Since filaments/prominences have been observed in the corona, the question arises about the mechanism which allows cool matter to be maintained during several solar rotations in the hot environment. A relatively simple answer to this question is the existence of a magnetic support. Two kind of magnetic models do exist for prominences to explain the support of their mass against the gravity: the wire model (Martin and Echols 1994) and the flux tube model. Cool material would be condensed in dips of magnetic fields. Using the idea of magnetic dips, Aulanier and Démoulin (1998) modelled realistic three-dimensional magnetic configurations with a linear force-free field (lfff) extrapolation and produce the morphology of filaments. According to the models, barbs represent cool

matter residing in small dips formed above the secondary photospheric inversion lines around parasitic magnetic elements which have the opposite polarity than the dominant polarity. More recently van Ballegoijen (2004) studied a barb of a U-shaped filament and found that the barb was associated with a weak network of major polarity using a non-lfff magnetic model. The corresponding models can explain the prominence fine structures as densified plasma lying in magnetic dips. Although such dips seem to be consistent with the few measurements of the magnetic field vector in prominences (Bommier *et al.* 1994). Recent investigations (Lopez *et al.* 2006) show the presence of dips in filament channels from THEMIS observations of the magnetic field vectors.

6. Conclusion

Multi-wavelength observations allow us to test models either dynamical or magneto-hydrodynamical models. Magnetic field in the corona can not be measured yet and is known by extrapolation and fitting the extrapolated loops with observed coronal loops (SOHO/EIT, TRACE). It is difficult to interpret a coronal or heliospheric event without knowing where it comes from. Its magnetic source region is an important key to explain the physical mechanism. Vector magnetograms are suitable for such studies. In this frame new instrumentations like SOLAR B, SDO will bring the answer to many questions.

References

- Aulanier G., Démoulin P., Schmieder B., Fang C., Tang Y. 1998, *Solar Phys.* 183, 369
 Aulanier G., Pariat E., Démoulin P. 2005, *A&A*
 Aulanier G., Schmieder B. 2002, *A&A* 386, 1106
 Aulanier G., Démoulin P. 1998, *A&A* 329, 1125
 Berlicki A., Schmieder B., Vilmer N., Aulanier G., DelZanna G. 2004, *A & A* 423, 1119
 Bommier V., Degli'Innocenti E., Leroy J.C., Sahal S. 1994, *Solar Phys.* 154, 231
 Démoulin P., 2005, Lindau, ESA conference
 Démoulin P., Bagala L., Mandrini C., Hénoux J.C., Rovira M. 1997, *A&A*, 325, 305
 Démoulin P., Priest E.R., Lonie D.P. 1996, *JGR*, 101, 7631
 Démoulin P., Mandrini C.H., Rovira M.G., Hénoux J.C., Machado M.E., 1994, *Solar Phys.* 150, 221
 Fan Y., Gibson S. 2004, Living review in Solar Physics, Editor S. Solanki
 Heinzel P., Farnik F., Anzer U., Dammasch I 2006, ASP, Solar B workshop, in press
 Khan J.I., Vilmer N., Saint-Hilaire P., Benz A. 2002, *A&A* 388, 362
 Kucera T., Andretta V, Poland A. 1998, *Solar Phys.* 183, 107
 Lin J. & Forbes T. 2000, *JGR* 105, 2375
 Lopez A., Aulanier G., Schmieder B., Sainz A.D. 2006, *A&A*, in press
 Mandrini C., Démoulin P., Schmieder B., *et al.* 2006, *A&A*, in press
 Martin S. & Echols, C. 1994, *Solar Surface Magnetism*, Dordrecht, Kluwer, 433, 303
 Pariat E., Aulanier G., Schmieder B., Rust D. *et al.* 2004, *ApJ* 614, 1099
 Pick M., Malherbe J.C., Kerdraon A., Maia D. 2005, *ApJ* L631, 97
 Saint Cyr C., Webb D.F. 1991, *Solar Phys.* 136, 379
 Schmieder B., van Driel L. 2004, *Proceedings of IAU S226*, Beijing, 149
 Schmieder B, Forbes T., Malherbe J.C., Machado M. 1987, *ApJ* 317, 956
 Schmieder B, Aulanier G., Démoulin P. 1997, *A&A* 325, 1213
 Subramanian P, Dere K. 2001, *A&A* 561, 372
 Sui L. & Holman G.D. 2003, *ApJ* 596, L251

van Ballegooijen A. 1994, ApJ 612, 519

Vilmer N., 2006, Proceedings of the Third French Chinese meeting, in press

van Driel L., Mandrini C., Schmieder B. *et al.* 1999, ASP Conf Series 184, 302

Webb D.F. 1998, in IAU Colloquium 167, ASP 150, 463

Zhou G, Wang J.X., Cao Z.L. 2003, A&A 397, 1057